ELSEVIER

Journal of Atmospheric and Solar-Terrestrial Physics 67 (2005) 259–268

Journal of ATMOSPHERIC AND SOLAR-TERRESTRIAL PHYSICS

www.elsevier.com/locate/jastp

The detectability of infrasound in The Netherlands from the Italian volcano Mt. Etna

L.G. Evers*, H.W. Haak

Seismology Division, Royal Netherlands Meteorological Institute, KNMI, P.O. Box 201, 3730 AE De Bilt, The Netherlands

Received 11 September 2003; received in revised form 11 May 2004; accepted 21 September 2004
Available online 26 November 2004

Abstract

Infrasound from the eruptions of Mt. Etna was detected in The Netherlands at the Deelen Infrasound Array (DIA) during the summer of 2001. Zonal cross winds lead to a deviation in the observed back azimuth. An average azimuthal deviation of 2.6° is explained by westward stratospheric winds along the infrasonic trajectories through the atmosphere. The signals have signal-to-noise power ratios lower than 0.6. The detectability of Mt. Etna's infrasound is tested on sub-arrays of the 13 elements of DIA. Doing so, sparse arrays used in the International Monitoring System (IMS) are mimicked. Both small aperture sub-arrays of 800 m and large aperture sub-arrays of 1400 m are applied. The results are evaluated on the basis of the number of detections made. The number of detections strongly increases with the number of elements. Small aperture sub-arrays perform significantly better than large aperture sub-arrays. With a factor of two reduction in the aperture, two instruments less can be used to obtain the same number of detections. Larger aperture arrays perform less well because of the loss of spatial coherence of the infrasound. The average accuracy of the detections slightly increased, when the number of elements is increased. The result of the use of more elements is that lower signal-to-noise power ratio events could be detected. The trade-off between more detections and the larger average deviation in back azimuth and apparent sound speed causes the slight increase accuracy. The results were comparable to the detections obtained at IMS array IS26 in Germany. It is concluded that successfully applying infrasound as monitoring technique strongly depends on the array configuration. The frequency versus spatial coherence of signals will play a decisive role in detecting low signal-to-noise ratio events.

Keywords: Infrasound; Arrays; Volcano; CTBT; Signal processing

1. Introduction

The lowest acoustical frequency resolved by humans is about 20 Hz. Inaudible sound or infrasound has frequencies lower than this threshold. The lower frequencies for infrasound are limited by the thickness of the atmospheric layer. Therefore, the infrasonic frequency band is defined between 100 s and 20 Hz.

Huge mass displacements in the atmosphere, like those caused by volcanic eruptions or nuclear tests, generate infrasound and can be detected at ranges of thousands of kilometres. The early period of infrasound developments came to an end with the Limited (Partial) Test Ban Treaty in 1963 that forced states to conduct nuclear tests underground. In recent years, since the signing of the Comprehensive Nuclear-Test-Ban Treaty (CTBT), infrasound research has been expanding again.

*Corresponding author. Tel.: +31 30 2206335; fax: +31 30 2201364.
E-mail address: evers@knmi.nl (L.G. Evers).

1364-6826/$ - see front matter © 2004 Elsevier Ltd. All rights reserved.
doi:10.1016/j.jastp.2004.09.002

Sixty infrasound arrays are currently being installed world wide as part of the International Monitoring System (IMS) for verification of the CTBT (PrepCom, 1997).

Infrasound from volcanoes measured in the far field is capable of penetrating the atmosphere over large ranges because of its low frequency content, i.e. between 0.5 and 2 Hz (Liszka and Garcés, 2002). Near-field measurements of infrasound from volcanoes give information about tremor sources, conduit and melt properties (Ripepe et al., 1996; Garcés et al., 2000).

The detection of infrasonic signals with arrays is based on signal coherence. Signal coherence decreases with increasing inter-array element distance (Mack and Flinn, 1971) while higher resolution might be achieved with larger aperture arrays. The resolution performance of an array also depends on the position of the instruments (Haubrich, 1968). The larger the array aperture, the lower the resolved frequencies.

In this paper, we investigate the detectability of infrasound from the 2001 Mt. Etna eruptions, in Italy, at the Deelen Infrasound Array (DIA) in The Netherlands. The influence of zonal cross winds on the recorded back azimuth is analysed. Furthermore, the number of sensing elements from DIA are systematically lowered from 13 to 4 to mimic sparse IMS arrays, like the 5 element array IS26 in Germany.

2. Infrasound data acquisition and processing

2.1. The Deelen Infrasound Array and IMS array IS26

Infrasound is monitored with arrays of microbarometers. Arrays are deployed to increase the detectability of signals as signal-to-noise ratios are often lower than 1. Signal stacking enhances the signal-to-noise ratios. Furthermore, information on the signal's back azimuth, ϕ, and apparent (horizontal) sound speed, $\vec{c}$, can be derived by applying array processing techniques. Spatial noise reducers are coupled to each instrument to further reduce noise caused by wind in an analog manner (Hedlin et al., 2003).

DIA is equipped with 16 KNMI differential microbarometers and capable of measuring events of CTBT interest (Evers and Haak, 2001b). Spatial noise reduction at each sensor is achieved by using 6 porous hoses. These are configured in a spider form, being a radial layout of the hoses, with a total diameter of 10 m. DIA has an aperture of approximately 1400 m and is located in the eastern part of The Netherlands on an Air Force base. This non-IMS array is used to perform sonic boom monitoring and CTBT related research. Fig. 1 gives the configuration of DIA as shown by the circles. Instruments 06, 08 and 09 were not operational at the time of the Etna eruptions in the summer of 2001.

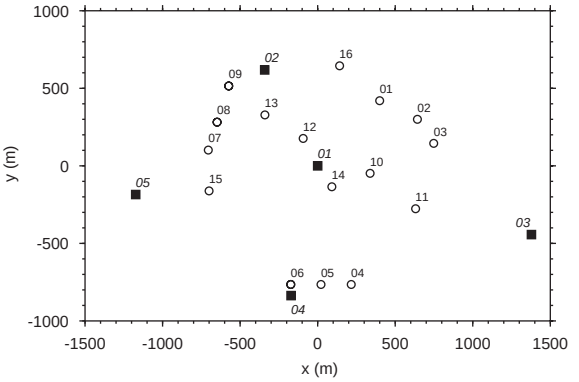

Fig. 1. The layout of 16 KNMI microbarometers of DIA (circles) and the 5 MB2000s of IS26 (filled squares, oblique numbers). Instruments 06, 08 and 09 of DIA were not operational.

IMS array IS26 in located in the Bavarian Forest in Southern Germany. IS26 consists of 5 absolute microbarometers (type: MB2000) and noise reduction is done with a metal pipe array of 18 m diameter at each sensor. The atmosphere is sampled with a total of 96 inlets connected to pipe array's 4 arms (Hartmann and Henger, 2000). The filled squares in Fig. 1 give the configuration of IS26.

2.2. Signal detection on the basis of the Fisher ratio

Array processing techniques are based on signal coherence. Detection algorithms trigger on specific threshold values, being for example: signal-to-noise ratio, correlation, coherency, LTA/STA. Evaluation of the Fisher ratio is another approach to find a systematic pattern in array data. Melton and Bailey (1957) defined the Fisher ratio as

$$F = \frac{T(N-1)}{N(T-1)} \frac{\sum_{t=1}^{T}(\sum_{n=1}^{N} X_{nt})^2 - (1/T)(\sum_{t=1}^{T}\sum_{n=1}^{N} X_{nt})^2}{\sum_{t=1}^{T}\sum_{n=1}^{N} X_{nt}^2 - (1/N)\sum_{t=1}^{T}(\sum_{n=1}^{N} X_{nt})^2}, \quad (1)$$

where the variances of N independent observations of quantity X are evaluated over a timespan T. The F-ratio is the ratio of "between sub-sample variance" to "within sub-sample variance". Basically, the recordings contain a part which can be attributed to a common cause as well as deviations not having the same origin. The "between sub-sample variance" contains both signal and noise power while the "within sub-sample variance" consists of noise power. Therefore, the F-ratio is a scaled measure of coherent signal-to-noise power ratio and describes the signal likelihood. The F-ratio is evaluated for a variety of incoming angles and apparent sound velocities of the energy, i.e. beamforming as commonly used in seismology (Blandford, 1974). This evaluation is done on a slowness, $\vec{p}$, grid where $\vec{p} = \hat{n}/\vec{c}$ with $\hat{n}$ being

the normal vector to the wavefront. A grid search is performed to find the $\vec{p}$ value which explains the observed travel time differences over the array, resolving ϕ and $\vec{c}$ as event characteristics.

3. Volcanic infrasound from Mt. Etna

3.1. Detections at DIA and IS26

Mt. Etna on the island of Sicily (Italy) violently erupted during the summer of 2001. Infrasound from explosions and huge mass displacements in the atmosphere were recorded at DIA and IS26. Although Mt. Etna was almost continuously active, data from two days of intense activity, being July 28 and 29, is concentrated on. Fig. 2 gives the results for the *F*-ratio analysis of 24 h of infrasound recorded at DIA and IS26 starting on 2001, July 28 12h00 GMT (local time-2h). The data for both arrays are bandpass filtered with a second order Butterworth filter having corner frequencies of 0.3 and 4.0 Hz. The *F*-ratio is evaluated on a $\vec{p}$ grid of 100×100 points forming 10.000 beams. The 24 h recordings are split up in bins of 25.6 s overlapping 50%. The lower frames in Fig. 2 give the maximum value for the *F*-ratio in each bin. The corresponding values for $\vec{c}$ and ϕ are given in the middle and top frames, respectively.

F-ratio values for DIA hardly show any infrasonic events during the day and early evening of July 28. The *F*-ratio increases around 21 h. Coherent infrasound is detected as also indicated by the apparent sound speed velocity which converges to sound speed values. The reason for the sudden increase in *F*-ratio is twofold.

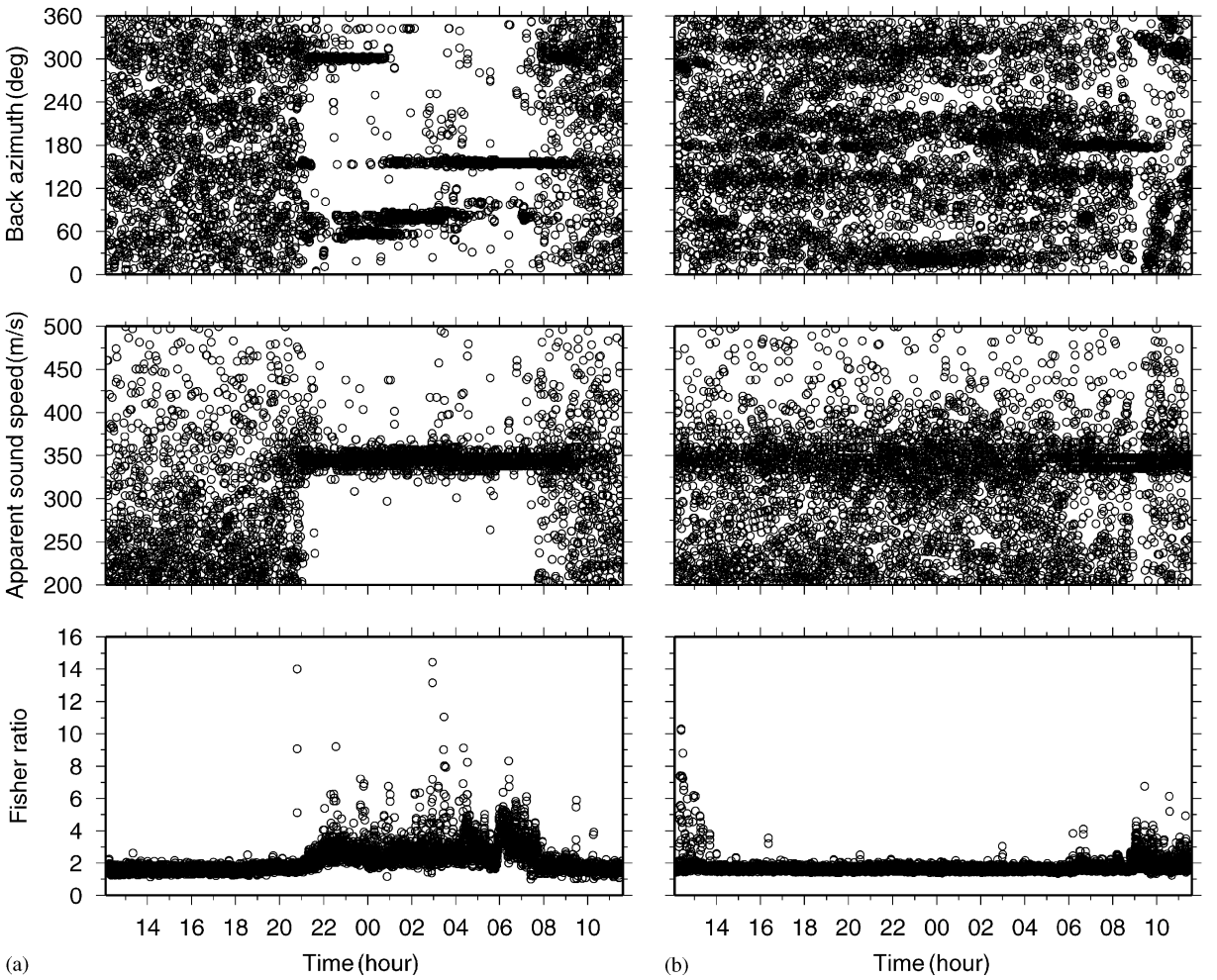

Fig. 2. *F*-ratio analysis of 24 h of infrasound recorded in DIA (a) and IS26 (b), the time axis starts on 2001, July 28 12h00 GMT. The maximum *F*-ratio is plotted in the lower frame for each time bin of 25.6 s, the corresponding values for $\vec{c}$ and ϕ are plotted in the top two frames.

Firstly and most importantly, the atmosphere becomes more stable after sunset, turbulent and convectional structures are no longer activated by solar heat fluxes. Secondly, noise around the array becomes less during the evening and night since human activity diminishes. The top frame of Fig. 2(a) shows three distinct directions from which the infrasound is coming towards DIA. A stable source is present to the Northeast of DIA at 300° between 21 and 1 h on the next day. Oceanic waves interacting with the atmosphere are the source, called microbaroms (Posmentier, 1967), and are located in the Atlantic Ocean (Evers and Haak, 2001b). A less well defined source is present eastwards of DIA. Between 21h and 4h30 a source seems to wander from 55° toward 85°. This energy is attributed to a local source because of its unstable character, no further explanation can be given for this source. A persistent back azimuth with an average value of $155.3 \pm 0.1°$ is resolved from 00h until at least 09h. This back azimuth is in the direction of Mt. Etna. The average apparent sound speed is found to be 340.6 ± 0.3 m/s. The total number of detections used to calculate these averages is 973. A detection of Mt. Etna is defined as an arrival with a F-ratio higher than 2 within a time segment of 25.6 s. The azimuth variation may be between 7° West and 3° East around the true back azimuth and an apparent sound velocity between 180 and 480 m/s is acceptable. The tolerance can be set much sharper as will be seen in the next sections.

Data from IS26, Fig. 2(b), appear more noisy. The stable and quiet nightly atmosphere does not result in the detection of coherent infrasound on the 5 element array. On the contrary, sources of infrasound are present during daytime. A stable back azimuth is visible between 06h and 10h on the morning of July 29, especially pronounced during a quiet moment around 09h. Its average back azimuth of $178.4 \pm 0.1°$ points towards Mt. Etna, the corresponding apparent sound speed is 341.7 ± 1.1 m/s. These averages are taken over 184 detections.

3.2. Azimuthal deviations

The true back azimuths for DIA and IS26 are 152.7° and 174.9°, respectively. Compared to the observed back azimuths an azimuthal deviation of 2.6° at DIA and 3.5° at IS26 is found. Fig. 3 shows these azimuthal deviations with respect to Mt. Etna. The origin of the infrasound found by cross bearing is located to the West of Mt. Etna.

Infrasonic wave propagation through the atmosphere is in first-order dependent on the wind and temperature structure. Raytracing through a moving atmosphere is conducted following the tau-p method described by Garcés et al. (1998). Infrasound travels through the atmosphere up to thermospheric heights. A model describing the wind and temperature structure up to these heights is provided by Hedin et al. (1996). This so-called HWM/MSISE model is taken at the halfway position of 10°E, 45°N on 2001, July 29 at 06h GMT, to get an indication of the azimuthal deviation. Although, lateral variations between Mt. Etna and DIA exist in the models, infrasonic paths will mainly be influenced by stratospheric zonal cross winds which are similar over Europe, justifying the use of the halfway model. Fig. 4 shows the results for raytracing from Mt. Etna towards DIA through the HWM/MSISE model. The paths the rays follow, lower frame of Fig. 4(a), either bend in stratosphere or thermosphere. Especially, thermospheric returns are split in several branches originating from heights between 110 and 130 km. The corresponding travel times are shown in the top frame of Fig. 4(a). The first energy to arrive in DIA is from stratospheric origin, subsequently low to high thermospheric returns arrive. It takes the energy, on average, 2 h to travel to DIA. Fig. 4(b) shows the bounce points on the Earth's surface for rays shot in the direction from Mt. Etna to DIA. It follows that rays do not arrive at DIA because of zonal cross winds deviating the rays towards the West. Stratospheric winds cause the deviation and have an east to west direction during summer, with speeds over 50 m/s at around 60 km height. Rays that will arrive at

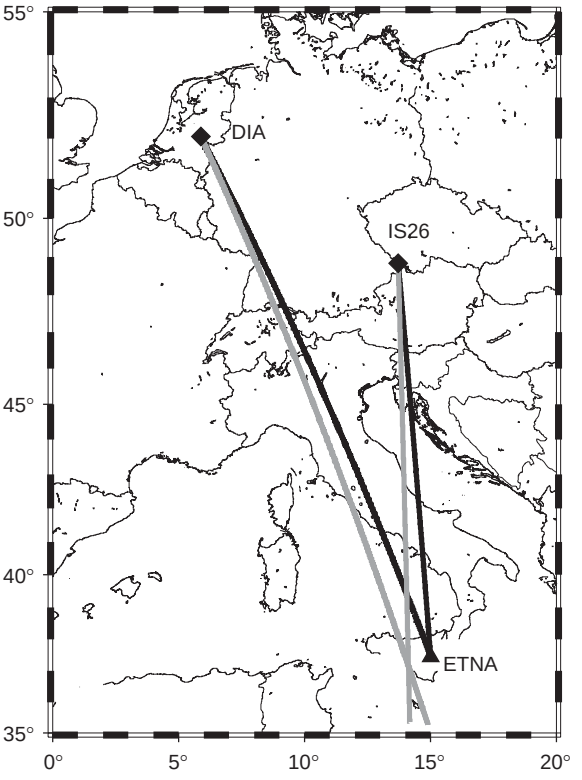

Fig. 3. Map showing the observed back azimuths (in grey) and true values (in black) from DIA and IS26 towards Mt. Etna.

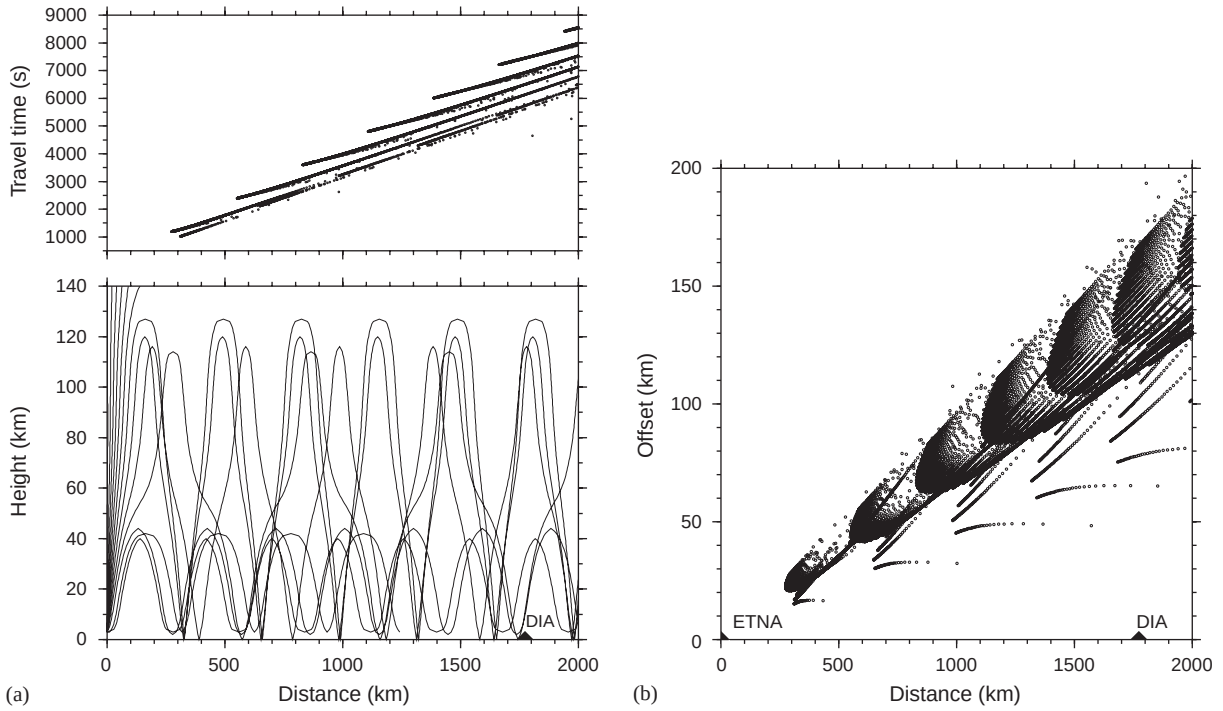

Fig. 4. The atmospheric trajectories and travel times as follows from raytracing from Mt. Etna towards DIA. The effective sound speed is calculated on the basis of HWM/MSISE models. (a) The bounce points of the rays on the Earth's surface (b) for rays shot from Mt. Etna in the direction of DIA. The rays are deviated westwards under the influence of zonal stratospheric cross winds.

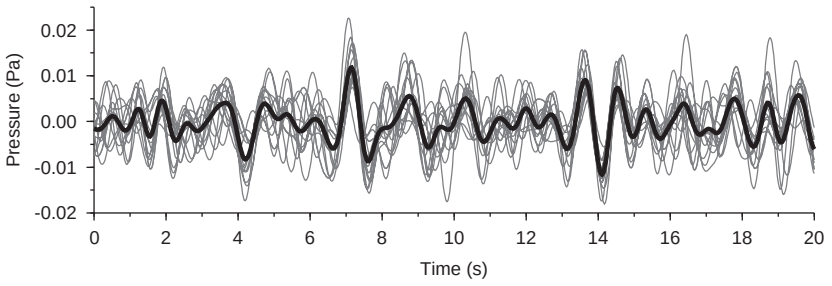

Fig. 5. Individual recordings of the 13 microbarometers of DIA in grey, the best beam in black. The time axis start at 06h14m38.8s on 2001, July 29 GMT. A second order Butterworth filter is applied with corner frequencies of 0.5 and 1.5 Hz.

DIA have to leave Mt. Etna is a more Easterly direction leading to a translation of the wavefront. This translation causes the observed azimuthal deviations and can range from 2° to 5°, see Fig. 4(b).

3.3. Infrasonic waveforms from Mt. Etna

Infrasound from Mt. Etna is recorded at DIA for at least 9 h. A wide variety of signal-to-noise power ratios are detected as indicated by the alternating *F*-ratio values, see Fig. 2(a). Distinct events, i.e. sub and supersonic airplanes, give rise to high *F*-ratios throughout the data set. The most coherent waveforms from Mt. Etna are detected between 06h and 07h during the morning of July 29. One of the highest *F*-ratios from Mt. Etna's infrasound is 9 corresponding to a signal-to-noise power ratio of 0.6. Fig. 5 shows the individual recordings around the time of the highest *F*-ratio in thin grey lines. These recordings are time aligned in the direction of Mt. Etna. The best beam, i.e. sum of the individual recordings, is shown as the black line. Infrasound from Mt. Etna can be identified there where the individual waveforms constructively add up in the best beam, see for example around 7 and 14 s. On the

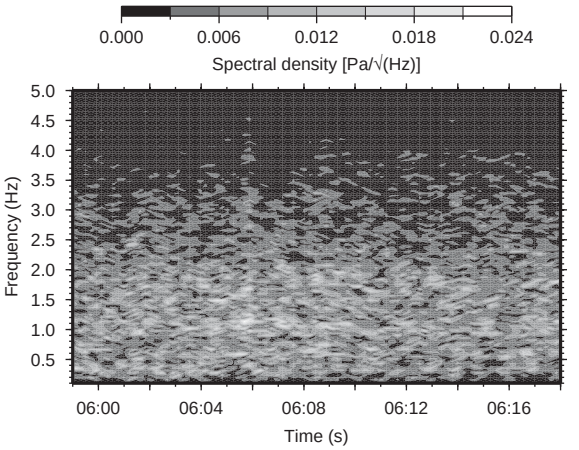

Fig. 6. Spectrogram for the best beam for Mt. Etna starting at 05:59 on 2001, July 29 GMT. The data are prefiltered with a second order Butterworth filter having corner frequencies of 0.3 and 4.0 Hz. The spectrogram is calculated for time bins of 25.6 s (1024 samples) with a 50% overlap, resolving spectral densities each 0.039 Hz.

other hand, noise is identified as non-coherent waveforms hardly contributing to the best beam, for example around 12 and 17 s.

The spectral contents of the best beam towards Mt. Etna is displayed in Fig. 6. The spectrogram shows spectral densities contoured for each 0.039 Hz as derived from time bins of 25.6 s (1024 samples). The dominant frequencies contributing to the best beam appear between 0.4 and 1.5 Hz as denoted by the light colors. An average frequency content of 1 Hz follows from a closer inspection of the actual waveforms.

4. The detection capability of sub-arrays of DIA

4.1. Number of detections

IS26 detected less energy from Mt. Etna than DIA, although, IS26 is situated 500 km closer to the volcano, see Fig. 2. There can be several explanations why IS26 seems to be less sensitive. Firstly, IS26 could have less sensitivity or more noisy instruments. Tests at the authors' institute have shown a comparable noise level and sensitivity for both instruments. The noise levels are low compared to the ambient noise in the atmosphere. Secondly, local noise levels could significantly differ at both arrays. IS26 is located in the forest which reduces the noise because the vegetation does not allow large turbulent structures to exist and also refracts the wind field. On the other hand, DIA is located on an open field and is thus more affected by turbulence and wind. The noise level in DIA is, therefore, expected to be higher which should result in fewer detections. Thirdly, the array layout from IS26 differs in both configuration and number of elements from DIA which may influence the number of detections. The last hypothesis is tested by assessing several sub-arrays of DIA. Two sets of sub-arrays are constructed of both small and large aperture. The large sub-arrays have a maximum aperture of 1400 m, see Fig. 7, while the small sub-arrays have a maximum aperture of 800 m, see Fig. 8. The sub-array layouts are chosen such that the array response has a circular and peaked main lob with low amplitude side lobes. This guarantees high resolution and omni-directional properties of the sub-array. Fig. 9 shows the number of detections made by sub-arrays of DIA as a function of the number of elements as circles for the large aperture sub-arrays and triangles for the small sub-arrays. The number of detections for IS26 is given as a square. Clearly, the number of detections increases with the number of elements. The small aperture sub-arrays perform significantly better than the large aperture sub-arrays. The loss of spatial coherence of the infrasound causes the decrease in number of detections with large aperture arrays. There is an almost linear increase in the number of detections with the number of elements for small aperture sub-arrays. For large aperture sub-arrays, the largest gain in number of detections is indicated by the steepest part of the curve between 7 and 9 elements. Further increase of the number of elements seems to lead to saturation. The saturation effect is also partly controlled by the maximum number of detections possible; the amount of infrasound from Mt. Etna is limited. Significant increase is also seen between 3 and 6 elements in both aperture sub-sets, but arrays of less than 5 elements suffer from resolution loss due to spatial aliasing (Evers and Haak, 2001a).

4.2. Accuracy of the detections

Fig. 10 shows the accuracy of the detections as function of the number of elements, circles for the large aperture sub-arrays and triangles for the small aperture sub-arrays. The averages are calculated by comparing the detections made by the sub-arrays with the 13 element solutions. The lower frame shows the average deviation in the resolved back azimuth. The middle frame shows these results for the apparent sound velocity. The top frame shows the average signal-to-noise power ratio of the detected events. There is a slight trend of increasing accuracy in both apparent sound speed and back azimuth frames. The average signal-to-noise power ratio clearly decreases with an increase in number of elements. This explains why the velocity and back azimuth curves only show a slight increase in accuracy. The influence of noise increases by increasing the number of elements, causing less coherent arrivals to be detected as follows from the signal-to-noise power ratios that are lowered. These less coherent arrivals are

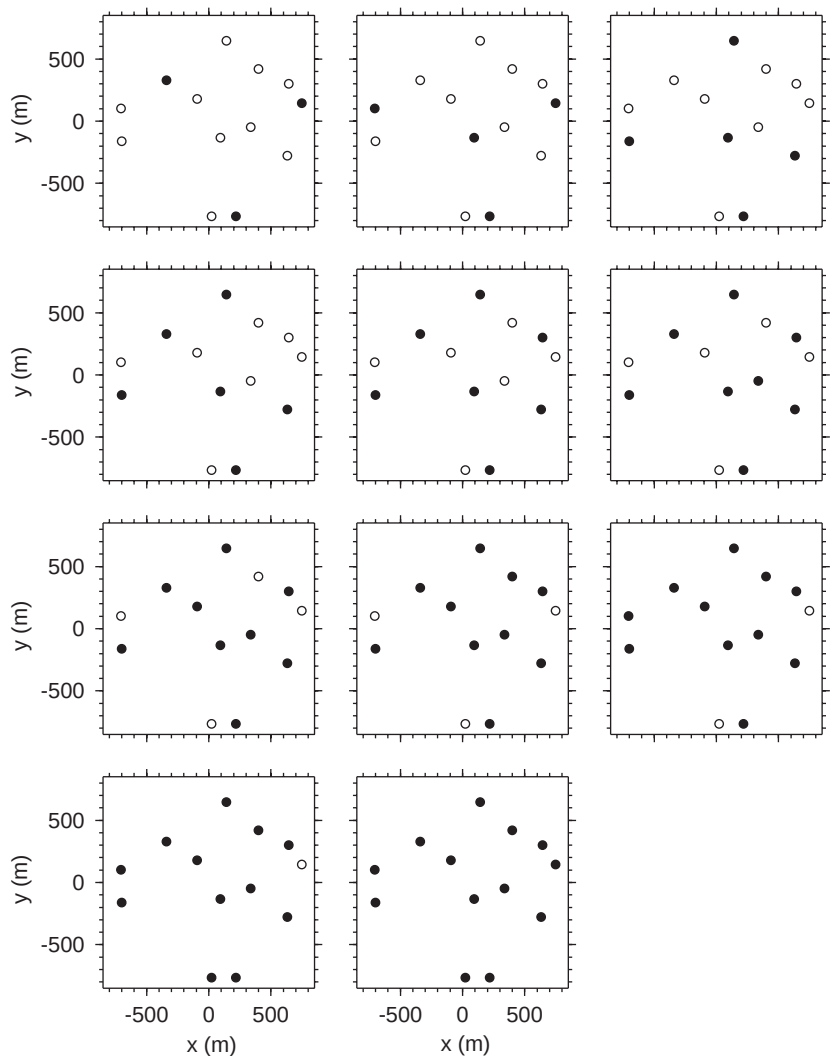

Fig. 7. Large sub-arrays of DIA with a maximum aperture of 1400 m. The elements used in the analysis are denoted by the filled circles. The number of active elements is increased from 3, upper left corner, to 13 in the lower right corner.

more difficult to characterize in terms of apparent sound speed and back azimuth. The spread in resolved values increases leading to larger standard deviation in the solutions. In general, the size of an array controls the accuracy of the derived back azimuth and apparent sound speed. Therefore, the large aperture sub-arrays appear to perform slightly better in terms of accuracy than the small aperture sub-arrays.

5. Conclusions

Infrasound from Mt. Etna has accurately been detected by the DIA in The Netherlands on 2001, July 28 and 29. The atmosphere becomes quiet and stable during the night enabling a clear identification of far-field volcanic infrasound. These ideal measurement conditions are due to minimization of the noise caused by human activity and the lack of solar heating. Daytime noise is partly generated by turbulent structures induced by heat fluxes. Energy that travels 1774 km from Mt. Etna to DIA is influenced by the wind and temperature structure of the atmosphere along its path. Impedance contrasts in the atmosphere lead to bending of the infrasonic rays in the stratosphere and thermosphere. Infrasound returns from approximately 40 km height in the stratosphere and several heights in the thermosphere between 100 and 130 km. Zonal cross winds explain the average 2.6° azimuthal deviation observed in DIA. Deviations are caused by westward

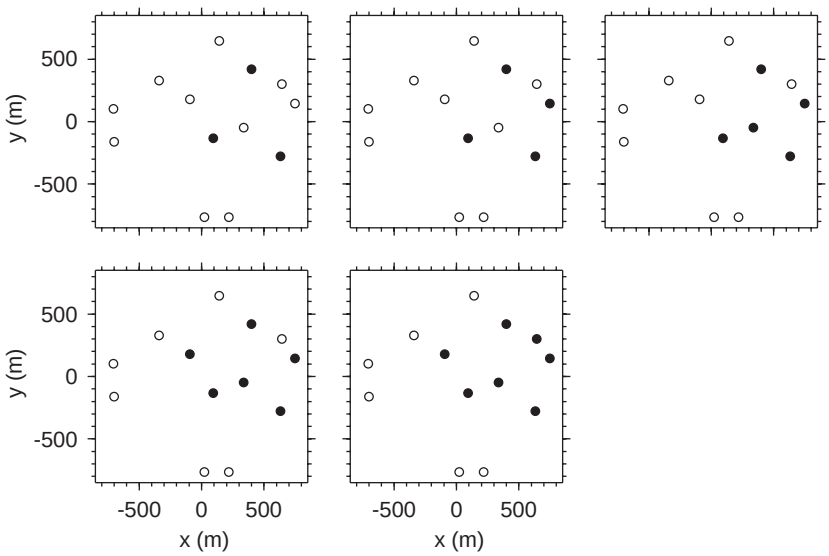

Fig. 8. Small sub-arrays of DIA with a maximum aperture of 800 m. The active elements, given by the filled circles, are increased from 3 to 7.

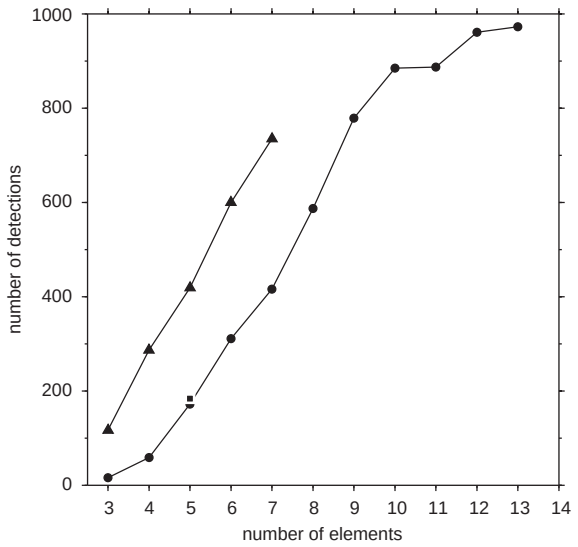

Fig. 9. Number of detections versus the number of elements for large aperture sub-arrays of DIA, circles, and IS26, square at 5 elements. The number of detections for small aperture sub-arrays are represented by the triangles.

winds in the stratosphere reaching over 50 m/s at 60 km height. The signals have low signal-to-noise power ratios, one of the most coherent waveforms has a signal-to-noise power ratio of 0.6. The detection capability of sub-arrays of DIA has been tested by lowering the number of active elements from 13 to 3 for small, 800 m, and large, 1400 m, aperture sub-arrays. The number of detections versus the number of elements is used as criterion. The two main findings are: small aperture sub-arrays perform much better than large aperture sub arrays and the number of detections strongly increases with the number of elements. With a reduction in size of the array with a factor of two, two instruments less to can be used to obtain the same number of detections. These findings are based on the observations and calculations made for volcanic infrasound specifically with a frequency content of 0.4–1.5 Hz. Increasing the number of instruments will slowly lead to saturation in the number of detections. This is also partly caused by the limited amount of detections that can be made. Larger aperture arrays perform less well because of the loss of spatial coherence of the infrasonic data. The average accuracy of the detections is only slightly improved. Increasing the number of element leads to the ability to detect signals with lower signal-to-noise power ratios but the detection of these events is less accurate. The trade-off between more detections and less accuracy causes the rather constant average deviation. Large aperture sub-arrays perform slightly better than small aperture sub-arrays in terms of accuracy. The obtained results are comparable to the detections obtained at the 5 element IMS array IS26 in Germany.

The detection capability of infrasound arrays is not only a function of the number of elements. The position of the instruments with respect to each other control the resolution and also the total aperture of the array. Therefore, the frequency versus the spatial coherence of the signals plays a decisive role in the chosen array layout and subsequently the success of infrasound as monitoring technique.

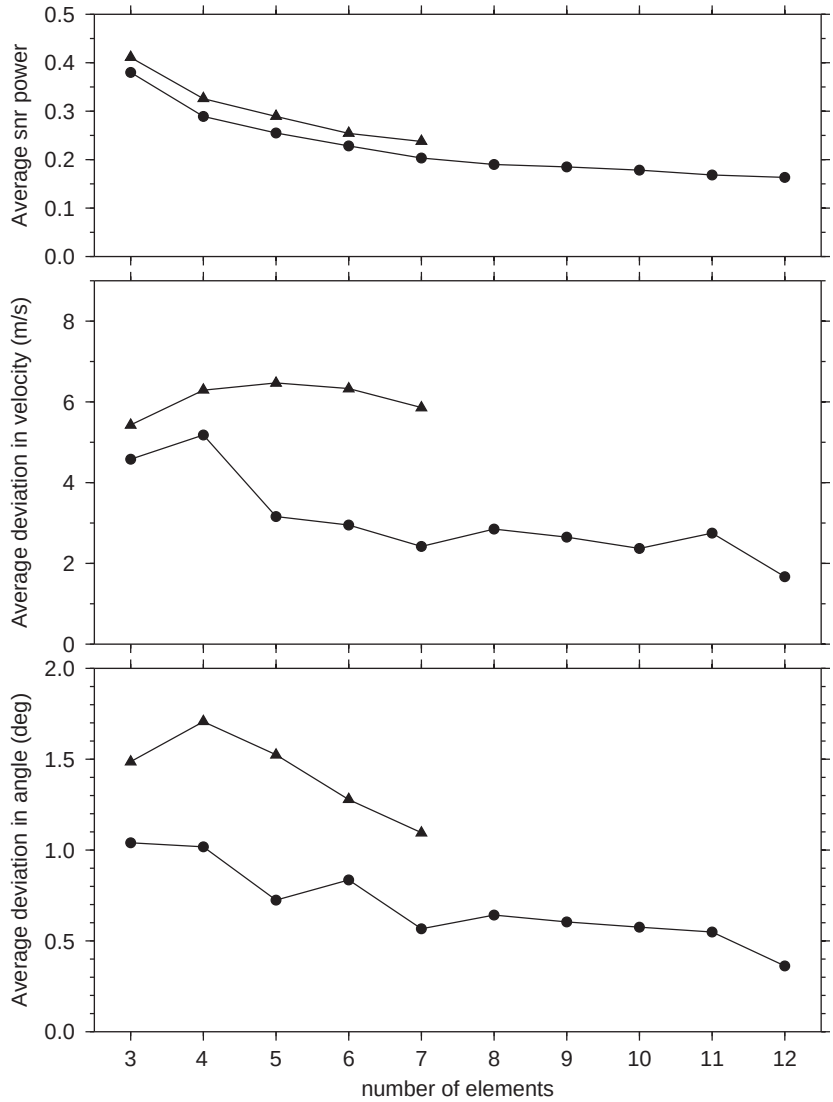

Fig. 10. The average deviation in back azimuth, lower frame, apparent sound velocity, middle frame and signal-to-noise power ratio, top frame, as function of the number of elements. The results for the large aperture sub-arrays are given by the circles, the triangles represent the small aperture sub-arrays.

Acknowledgements

The authors acknowledge the cooperation with the Royal Netherlands Airforce in DIA. David Norris is thanked for providing the HWM/MSISE models. Pictures in this article were made with the Generic Mapping Tool (Wessel and Smith, 1991).

References

Blandford, R.R., 1974. An automatic event detector at the Tonto Forest Seismic Observatory. Geophysics 39, 633–643.

Evers, L.G., Haak, H.W., 2001a. An Optimal Infrasound Array at Apatity (Russian Federation). KNMI-Publication 195, Royal Neth. Meteo. Inst., de Bilt, The Netherlands, 42pp.

Evers, L.G., Haak, H.W., 2001b. Listening to sounds from an exploding meteor and oceanic waves. Geophysical Research Letters 28, 41–44.

Garcés, M.A., Hansen, R.A., Lindquist, K.G., 1998. Travel times for infrasonic waves propagating in a stratified atmosphere. Geophysical Journal International 135, 255–263.

Garcés, M., McNutt, S.R., Hansen, R.A., Eichelberger, J.C., 2000. Application of wave-theoretical seismoacoustic models to the interpretation of explosion and eruption tremor signals radiated by Pavlof, volcano, Alaska. Journal of Geophysical Research 105, 3039–3058.

Hartmann, G., Henger, M., 2000. Milestones of the IS26 installation. Presented during the Infrasound Workshop 2000, Passau, Germany, October 2–6.

Haubrich, R.A., 1968. Array design. Bulletin of the Seismological Society of America 58, 977–991.

Hedin, A.E., Fleming, E.L., Manson, A.H., Schmidlin, F.J., Avery, S.K., Clark, R.R., Franke, S.J., Fraser, G.J., Tsuda, T., Vial, F., Vincent, R.A., 1996. Empirical wind model for the upper, middle and lower atmosphere. Journal of Atmospheric and Terrestrial Physics 58, 1421–1447.

Hedlin, M.A.H., Alcoverro, B., D'Spain, G., 2003. Evaluation of rosette infrasonic noise-reducing spatial filters. Journal of the Acoustical Society of America 114, 1807–1820.

Liszka, L., Garcés, M.A., 2002. Infrasonic observations of the Hekla eruption of February 26, 2000. Journal of Low Frequency Noise, Vibration, and Active Control 21, 1–8.

Mack, H., Flinn, E.A., 1971. Analysis of the spatial coherence of short-period acoustic-gravity waves in the atmosphere. Journal of the Royal Astronomical Society 26, 255–269.

Melton, B.S., Bailey, L.F., 1957. Multiple signal correlators. Geophysics XXII, 565–588.

Posmentier, E.S., 1967. A theory of microbaroms. Geophysical Journal of the Royal Astronomical Society 13, 487–501.

Preparatory Commission for the Comprehensive Nuclear-Test-Ban Treaty Organization (PepCom), 1997. Comprehensive Nuclear-Test-Ban Treaty (CTBT), V.97-28276, Austria, 139pp.

Ripepe, M., Poggi, P., Braun, T., Gordeev, E., 1996. Infrasonic waves and volcanic tremor at Stromboli. Geophysical Research Letters 23, 181–184.

Wessel, P., Smith, W.H.F., 1991. Free software helps map and display data. EOS Transactions AGU 72, 441.